Asian Journal of Chemistry; Vol. 37, No. 8 (2025), 1913-1926

ASIAN JOURNAL OF CHEMISTRY

https://doi.org/10.14233/ajchem.2025.34030

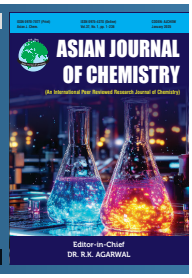

Rapid Green Synthesis of Ag-TiO_2 Nanocomposites *via* Microwave Irradiation for Water Treatment: Dual Action on Dyes and Bacteria

D. KANAKARAJU[1,*], D.N. JOSEPH[1], Y.C. LIM[2] and M. VINCENT[1]

[1]Faculty of Resource Science and Technology, Universiti Malaysia Sarawak, 94300 Kota Samarahan, Sarawak, Malaysia
[2]School of Chemistry and Environment, Faculty of Applied Sciences, Universiti Teknologi MARA, 40450 Shah Alam, Selangor, Malaysia

*Corresponding author: Tel: +60 82 583023; E-mail: kdevagi@unimas.my

Received: 12 May 2025; *Accepted*: 4 July 2025; *Published online*: 31 July 2025; AJC-22070

The widespread use of hazardous chemicals in traditional methods for synthesizing silver-doped titanium dioxide (Ag-TiO_2) nanocomposites poses significant environmental and health concerns, contradicting the goal of sustainable photocatalytic water purification. This study aims to develop a microwave-assisted green synthesis method using plant waste-based material, *Allium cepa* (onion) peel extract, a readily available material, to deposit silver onto TiO_2 with the goal enhancing its photocatalytic and antibacterial properties. The prepared Ag-TiO_2 nanocomposite was applied to remove single and mixed dyes. Characterization techniques confirmed the formation of stable Ag-TiO_2 nanocomposite with an average size of 7.36 ± 2.01 nm evenly deposited onto TiO_2, resulting in improved responsiveness in the visible light region. UV-Vis diffuse reflectance spectroscopy and photoluminescence analysis indicated a reduction in the band gap for Ag-TiO_2 nanocomposite. The green-synthesized Ag-TiO_2 nanocomposite exhibits exceptional photocatalytic efficiency in degrading both cationic dyes and anionic Congo red and methylene blue dyes with a degradation rate of 99.4% and 99.6% individually under UV irradiation. In a mixed dye solution, the degradation of rhodamine B and methyl orange dyes was significantly accelerated due to the selective interaction of the Ag-TiO_2 nanocomposite with anionic dyes. The green synthesized Ag-TiO_2 nanocomposite also showed effective antibacterial properties against Gram-positive bacteria, *E. coli* and Gram-negative bacteria, *S. aureus*. This study stresses the capability of green synthesis to generate environmentally benign and high-performing photocatalysts for water treatment applications, effectively degrading contaminants and eradicating undesirable waterborne pathogens.

Keywords: Photocatalysis, Green route, Doping, Water treatment, Emerging pollutants.

INTRODUCTION

Water contamination from a wide array of pollutant sources poses a substantial threat to human well-being and the environment, especially with continued population expansion and industrialization. Industries, such as textile, often utilize dyes like methylene blue, methyl orange, rhodamine B and Congo red due to their ease of application as colourings. However, about 15% of dyes remain unabsorbed during the dyeing process and are discharged as effluents, leading to water pollution [1]. Annually, around 12-14% of the 700,000 tons of dye used in industries are discharged into the environment, posing a severe risk to aquatic ecosystems [2]. These unabsorbed dyes are persistent and do not easily degrade in the water bodies, potentially contaminating drinkable water above permissible levels and causing health complications due to their carcinogenic properties [3-5]. Several strategies have been proposed to address this issue, including adsorption, bioremediation, membrane technology and photocatalytic degradation [6,7].

Extensive studies have focused on the photocatalytic degradation of dyes utilizing nanomaterial-based assemblies due to their simplicity, efficiency, utilization of renewable energy sources (sunlight) and capability to mineralize organic pollutants completely into non-hazardous compounds [8,9]. Titanium dioxide (TiO_2)-based nanomaterials are among the most widely studied photocatalysts due to their non-toxic nature, chemical stability and efficient charge separation, resulting in high photocatalytic activity [10]. However, the high energy band gap of pristine TiO_2 limits photoexcitation to the ultraviolet (UV) region, making it an ineffective photocatalyst. To tackle this limitation, various methods have been explored, including nanostructuring of TiO_2 and integration of co-catalysts or semicon-

ductors. One promising method is the deposition of noble metals like silver onto TiO_2, which enhances its performance within the visible light region through the surface plasmon resonance (SPR) effect [11].

Thus far, various strategies have been explored to synthesize Ag-TiO_2 nanocomposites (NCs), such as laser ablation, solvothermal and chemical reduction. Nevertheless, many of them involve the use of chemicals that produce toxic byproducts harmful to the environment [12,13]. Therefore, green synthesis, which employs plant extract-mediated reactions, has gained attention for its ability to induce chemical reduction and act as capping agents without producing toxic byproducts. While the specific phytochemicals involved in the green synthesis are not fully understood, studies have identified flavonoids, terpenoids, phenolics and steroids among the phytochemicals that participate in the synthesis mechanism [14,15]. Green synthesis also allows for precise control in producing high yields of nanomaterials with well-defined sizes and morphologies [16]. The Au-Ag-TiO_2 nanocomposites synthesized using *Cinnamomum camphora* leaf extract showed a well-defined spherical Au and Ag nanoparticles with sizes of 12.6 nm which could degrade approximately 90% of methyl orange within 30 min when exposed to UV-Vis light [17].

In comparison to previous studies that utilized green synthesis for the fabrication of Ag-TiO_2 NCs (Table-1), this study showed superior photocatalytic activity due to a more efficient synthesis method. Most of the earlier studies that used methylene blue as a model pollutant (Table-1) developed the relevant materials using facile plant-extract mediated synthesis methods. In contrast, the microwave technique used in this work has a number of benefits such as reduced total synthesis time and the fabrication of Ag-TiO_2 with a regulated morphology and uniform dispersion of Ag onto TiO_2. The microwave-assisted synthesis, mediated by onion peel extract, successfully yielded green material functionalized nanocomposites with enhanced photocatalytic activity. This study explored the green synthesis of Ag-TiO_2 NCs using *Allium cepa* (onion) extract, which is rich in flavonoids, terpenoids and phenolics that are crucial for the green synthesis reaction [23,24]. Hence, this study contributes to advancing green synthesis methods for producing efficient photocatalysts for environmental remediation.

TABLE-1
COMPARISON OF PHOTOCATALYTIC ACTIVITY FOR Ag-TiO_2 NANOCOMPOSITES

Dye	Type of plant extract	Degradation (%)	Ref.
MB	*Nephelium lappaceum* L. peel	81.0	[18]
MB	*Azadirachta indica* leaf	90.0	[15]
MB	*Mangifera indica* leaf	68.0	[19]
Rh B	*Cleistocalyx operculatus* leaf	91.4	[20]
MB	*Cucumis melo* juice	95.3	[21]
MB	*Garcinia mangostana* pericarp	96.7	[22]
MB	*Allium cepa* peel	99.6	Present work

This study also aimed to evaluate the structural and optoelectronic properties, as well as the photocatalytic and antibacterial performance of green-synthesized Ag-TiO_2 NCs through microwave irradiation. The photocatalytic activity was investigated using two cationic dyes, rhodamine B and methylene blue and two anionic dyes, Congo red and methyl orange as model pollutants. The performance of Ag-TiO_2 NCs in removing these dye pollutants was compared and their antibacterial properties were also assessed.

EXPERIMENTAL

Commercial anatase TiO_2 (99.8%), *p*-benzoquinone (BZQ), methylene blue (MB, 82%), methyl orange (MO, 85%), rhodamine B (RhB, >95%) and Congo red (CR, > 35%) were purchased from Sigma-Aldrich, USA. $AgNO_3$ (99.98%) was procured from Bendosen. Methanol (MeOH) was purchased from Merck, USA. Other reagents like 95% ethanol (EtOH) and hydrogen peroxide (H_2O_2) were purchased from HmbG Chemicals. *A. cepa* (onion) was bought from a local supermarket in Kuching, Sarawak, Malaysia. All solutions were prepared with distilled water and the chemicals involved in the overall process were used without further puri-fication.

Preparation of *Allium cepa* (onion) peel extract: The *A. cepa* (onion) peel extract was prepared according to the reported methods [25,26] with some minor changes. After obtaining the dried onion peel powder, 10 g of powder was mixed with 300 mL of 70% EtOH. The mixture was sonicated for 30 min, resulting in a dark red solution, which was allowed to cool to room temperature. Once cooled, the mixture was filtered to remove any remaining solid residues. The filtrate containing the onion peel extract was then kept in a refrigerator at 4 ºC for the green synthesis of Ag-TiO_2 NCs.

Green synthesis of Ag-TiO_2 NC: The green synthesis methods for Ag-TiO_2 NCs were modified from the published work [27,28]. Initially, 30 mL of onion peel extract was added dropwise to a 10 mL solution containing 1 g of $AgNO_3$ and the mixture was stirred magnetically for 30 min. The solution was then subjected to microwave irradiation at 100 W for 6 min. The resulting reddish-brown colloidal suspension of AgNPs was mixed with 1 g of TiO_2 in 10 mL of distilled water. The Ag-TiO_2 NC solution was poured into a Petri dish and oven-dried overnight at 70 ºC. The dried solid was scraped off with a spatula, ground into a fine powder and subsequently calcined at 300 ºC for 5 h. A control sample was prepared in the same manner but in the absence of the onion peel extract. The resulting powder was stored for characterization and photocatalytic degradation studies.

Characterization: The characterization of AgNPs, TiO_2 and Ag-TiO_2 NCs was done to obtain information about their physicochemical properties. Scanning electron microscopy (Model: JEOL, JSM-IT500HR) paired with energy dispersive X-ray (Model: JEOL, JSM-IT500HR) was used for the determination of morphological and elemental composition. The microstructural characteristics and particle dimensions of Ag-TiO_2 NCs were examined using a JEOL Model JEM 1230 transmission electron microscope (TEM). Analysis of functional groups present in the NCs was done *via* FTIR (Model: Thermo Nicolet iS10) using KBr pellets as a standard at the wavelength of 4000-400 cm^{-1}. X-ray diffraction analysis (XRD, PANalytical X'pert Pro) was also done to determine the crystalline structure

and phase of the green synthesized samples. UV-Vis diffuse reflectance spectroscopy (UV-Vis DRS, Model Carry 5000) was employed to determine the effective absorption spectra of Ag-TiO_2 NC and the Kubelka-Munk plot was established to confirm any changes in the energy bandgap of the Ag-TiO_2 NCs. Photoluminescence (Model: Perkin-Elmer LS55) emission spectra of the synthesized samples were done with a fluorescence spectrometer equipped with a xenon lamp at an excitation wavelength of 325 nm to gather information about the optoelectronic properties of the green synthesized Ag-TiO_2 NCs.

Photocatalytic experiments: The photocatalytic performance of the Ag-TiO_2 NC was investigated based on the dosage of photocatalyst, the concentration of MB dye and the comparative performance of the green synthesized Ag-TiO_2 NC, AgNPs and TiO_2 under UV and visible light. A 100 mL MB solution was prepared with varying concentrations of 5-15 ppm. Different concentrations of MB dye were treated with varying dosages of Ag-TiO_2 NC (0.1-1.0 g/L) in a 250 mL beaker to optimize the conditions for MB dye photodegradation. The suspension was stirred in the dark before hand to maintain Ag-TiO_2 NC suspension at equilibrium and allow the suspension to reach adsorption-desorption equilibria for 30 min. Then, it was continuously stirred with a magnetic stirrer under the irradiation of a UV lamp (λ = 365 nm) for 2 h. About 4 mL of suspension aliquots were withdrawn and centrifuged at 5,000 rpm for 10 min. The absorbance of the supernatant was analyzed using UV-Vis spectroscopy at 664 nm to evaluate the photo-catalytic degradation of MB dye. This procedure was repeated for TiO_2 and AgNP under similar conditions for photocatalysis using UV and visible light sources. The removal efficiency of MB dye was calculated as follows:

$$\text{Removal efficiency } (\%) = 1 - \frac{C_{final}}{C_{initial}} \times 100 \quad (1)$$

The photocatalytic experiments were performed using CR, MO and RhB dyes. The optimized condition of MB dye removal was applied for the other three dyes to compare the photocatalytic activity of the Ag-TiO_2 NC to degrade different cationic and anionic dyes. Consequently, the photocatalytic experiments were also done for mixed dye systems.

Given that MB dye had the maximum degradation, further study on stability and radical scavenger was assessed with MB dye as the model pollutant. Finally, the stability of Ag-TiO_2 NC was assessed by studying its photocatalytic efficiency in degrading freshly prepared 5 ppm of MB solution under four consecutive runs using a UV light source and optimized experimental conditions. Radical scavenger study was conducted using methanol (0.2 mmol/L), *p*-benzoquinone (0.2 mmol/L) and hydrogen peroxide (0.1 mmol/L) as inhibitors for holes (h^+), superoxide radicals ($^\bullet O_2^-$) and hydroxyl radical ($^\bullet OH$).

Antibacterial study: The antibacterial study was conducted using the disc diffusion method to determine the antibacterial efficiency of the Ag-TiO_2 NC against both Gram-positive bacteria, *E. coli* and Gram-negative bacteria, *S. aureus*. The bacterial strains were obtained from the Microbiology Laboratory 2, Faculty of Resource Science and Technology, UNIMAS. The bacterial strains were first, revived in nutrient broth (NB) and then inoculated onto nutrient agar (NA) plates. Next, the inoculum was standardized by transferring several colonies into fresh NB and adjusting the culture to a turbidity that is equivalent to 0.5 McFarland standard. The antibacterial assay was conducted by first comparing the effectiveness of Ag-TiO_2 against onion peel extract, TiO_2 and AgNPs to inhibit the growth of the bacterial samples. All samples were fixed to a concentration of 1 g/L. A fixed amount of sample was mixed in a phosphate buffer (PBS) solution. Sterile filter papers were then dipped into the PBS solution containing these samples. The standardized inoculum was subsequently swabbed onto NA plates using sterile cotton swabs. The treated filter papers were then placed on the agar surface and incubated at 37 ºC for 24 h. The diameter of the inhibition zones was measured after the incubation period. The experiment was repeated by varying the concentrations of the Ag-TiO_2 nanocomposite at 1, 2, 4, 8 and 10 g/L.

RESULTS AND DISCUSSION

Characterization: The FTIR spectrum depicted in Fig. 1 illustrates broad peaks observed at 3421 and 1628 cm^{-1}, corresponding to -OH stretching and -OH bending, respectively. In contrast to the -OH peak observed in commercial anatase TiO_2, Ag-TiO_2 NC exhibited a higher intensity of peaks. This enhancement can be attributed to the presence of phenolic compounds derived from onion peel extract, which become attached to the photocatalyst's surface during the green synthesis process. The characteristic peak observed at 1116 cm^{-1} indicates the presence of C=C aromatic rings confirmed that phytochemicals extracted from the onion peel extract remained attached to the surface of Ag-TiO_2 NCs. These naturally occurring compounds would have been responsible for the peaks observed through FTIR analysis. A noticeable shift in peaks from 1428 cm^{-1} (TiO_2) to 1394 cm^{-1} (Ag-TiO_2 NC) suggests the presence of the Ag-Ti bond, demonstrating successful deposition of Ag onto TiO_2 *via* onion peel extract-induced reaction. The low-intensity peak of Ag-O around 595 cm^{-1} [29] shows that phenolics from the onion peel extract prevent oxidation of AgNPs that are deposited onto the surface of TiO_2, thus forming stable green synthesized Ag-TiO_2 NC. The peaks at 613 cm^{-1} (Ti-O-Ti) [30] and the shift in peaks at 517 cm^{-1} for TiO_2 to 478 cm^{-1} for Ag-TiO_2 described the formation of pure AgNPs that have been loaded onto TiO_2 [31].

The surface morphology of the synthesized Ag-TiO_2 NC was gathered by SEM analysis. It was found that TiO_2 appears spherical with even dispersion (Fig. 2). In contrast, the SEM micrograph of the green-synthesized Ag-TiO_2 NC (Fig. 2c) shows monodispersed spherical AgNPs clustered on the surface of TiO_2. A similar SEM micrograph is observed for green synthesized AgNPs, whereby clusters of spherical AgNPs are attained (Fig. 2b). Additionally, TEM micrographs (Fig. 3a-b) reveal AgNPs with an average size of 7.36 ± 2.01 nm deposited onto TiO_2, representing the success of the doping process for Ag-TiO_2 NCs. The AgNPs exhibited a particle size distribution ranging from 2-21 nm (Fig. 3c). The formation of clustered particles is attributed to the binding capacity of various phytochemicals in the onion peel extract, which act as capping agents

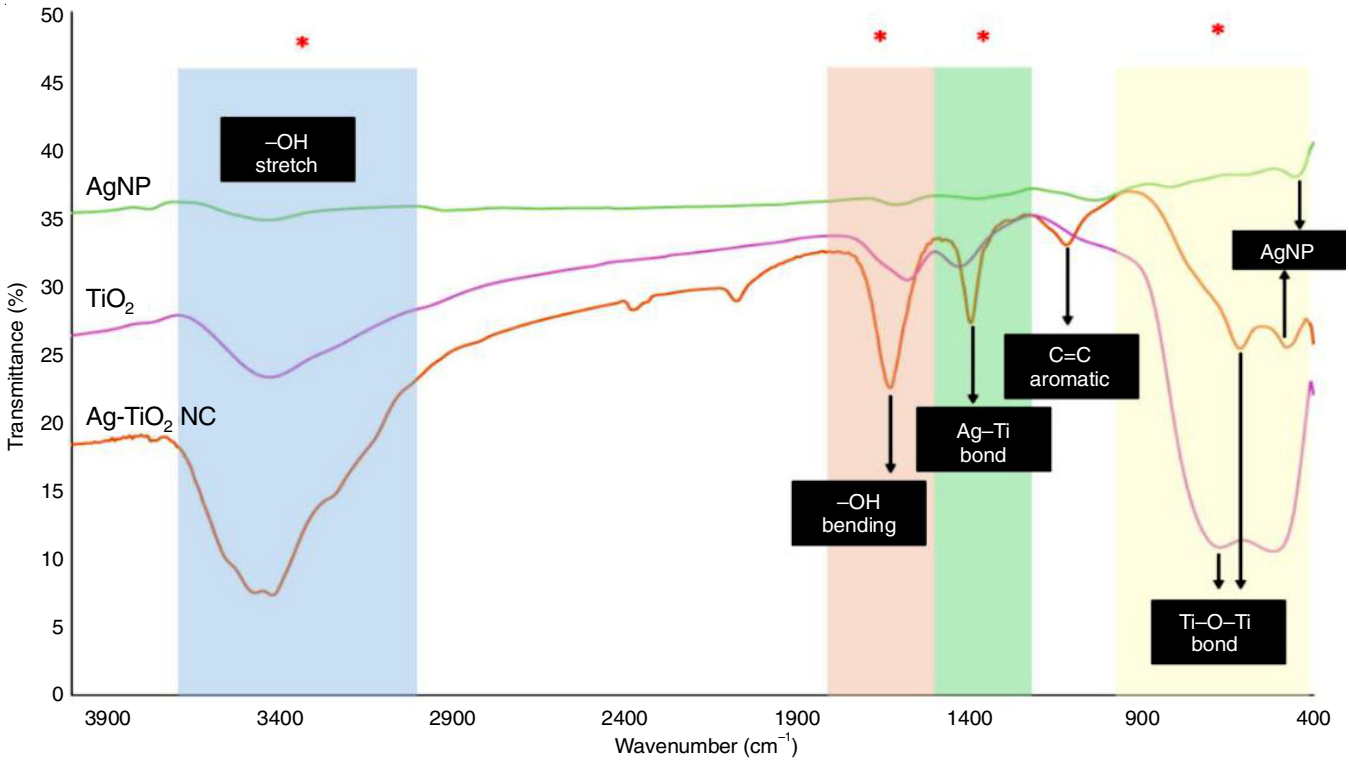

Fig. 1 FTIR spectra of AgNPs, TiO_2 and Ag-TiO_2 NC

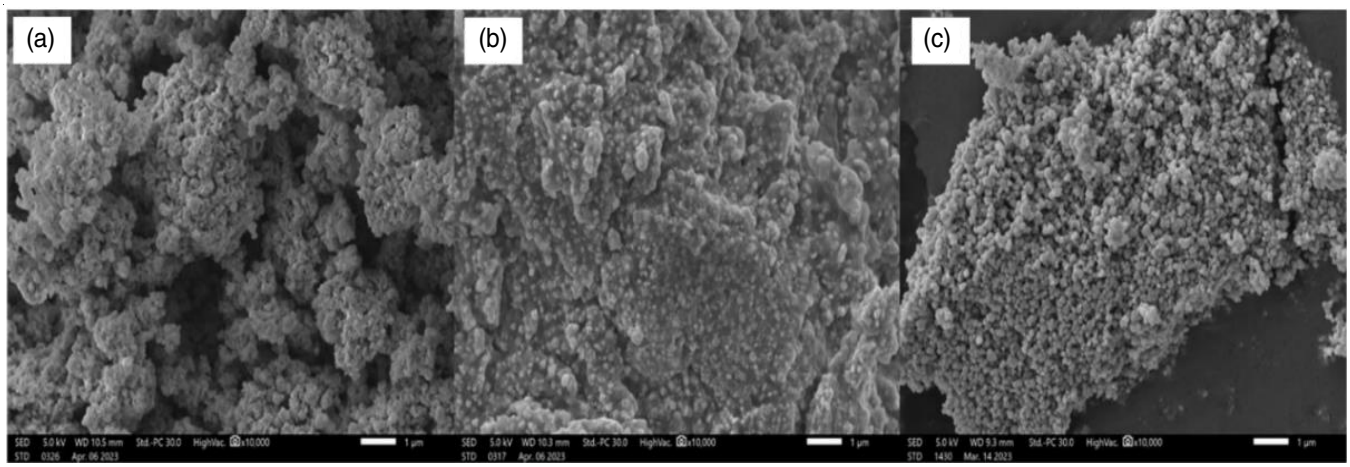

Fig. 2. SEM micrographs of (a) Ag-TiO_2 NC, (b) AgNPs and (c) TiO_2

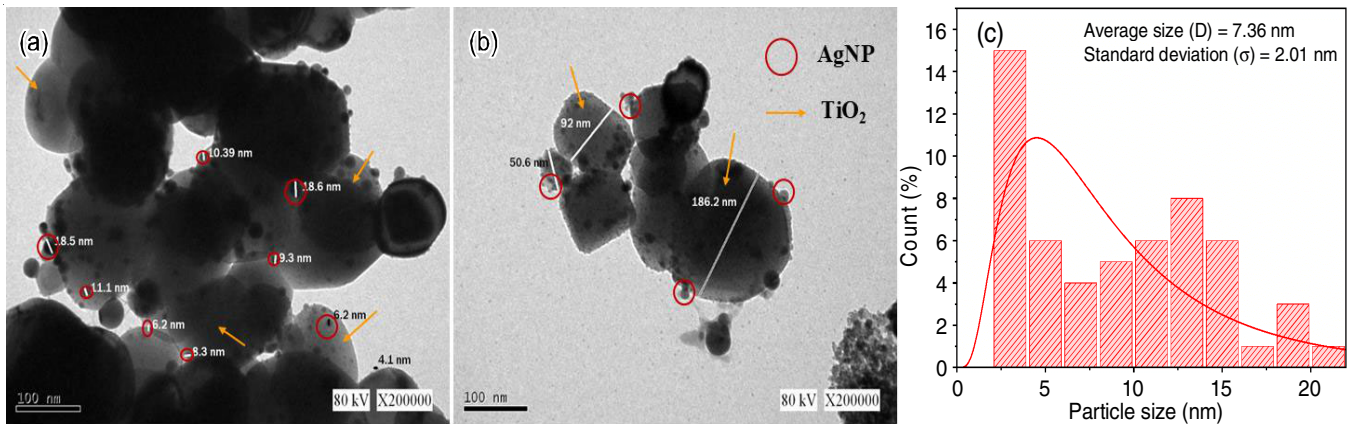

Fig. 3. TEM micrographs of Ag-TiO_2 NC (a,b) and particle size distribution of AgNPs fabricated onto TiO_2 (c)

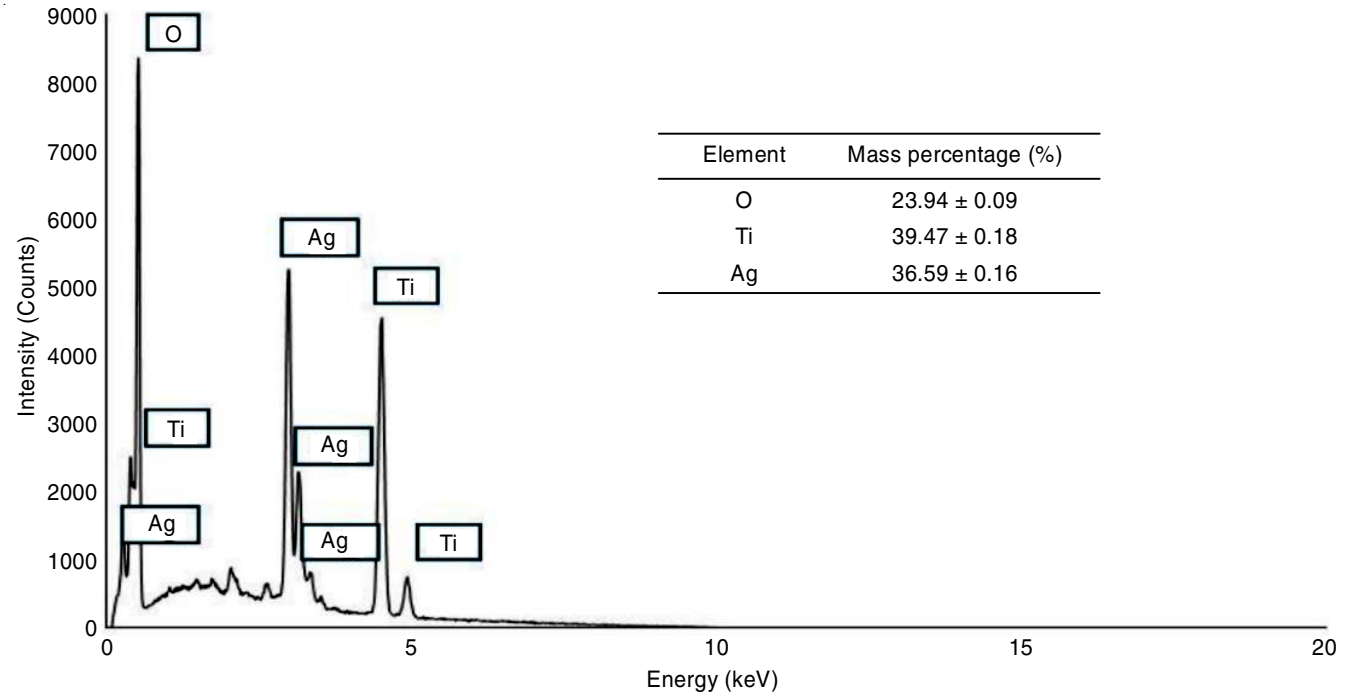

Element	Mass percentage (%)
O	23.94 ± 0.09
Ti	39.47 ± 0.18
Ag	36.59 ± 0.16

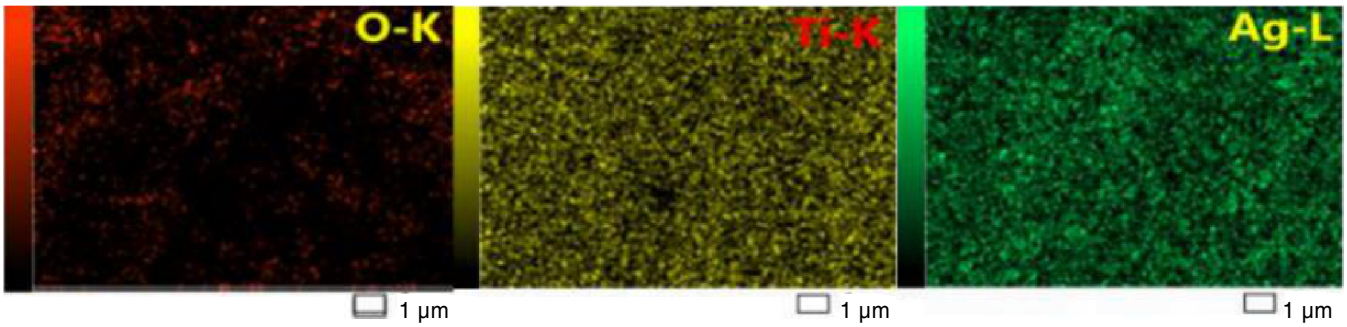

Fig. 4. EDX spectrum and mapping of Ag-TiO_2 NC

for the green synthesized AgNPs and Ag-TiO_2 NC [32]. Prior studies have reported that these phytochemicals act as a stabilizing agent to form particles with controlled morphology [33, 34], as revealed by the SEM micrographs.

The EDX analysis and mapping (Fig. 4a-b) depicts that the composition of Ag and Ti is approximately equal in mass, as the percentages of Ag, Ti and O are confirmed to be 36.59%, 39.47% and 23.94%. It indicates that the green synthesized Ag-TiO_2 NC adhered to the stoichiometric ratio that is approximately 1:1 for elements of Ag and Ti, proving the success of the synthesis with no detection of other impurities.

Fig. 5 depicts the XRD patterns of AgNPs, TiO_2 and Ag-TiO_2 NC. It can be observed that major anatase peaks are detected at 2θ 25.4º (101), 36.9º (103), 37.9º (004), 38.4º (112), 48.1º (200), 53.9º (105), 55.1º (211), 62.8º (204), 68.9º (116), 70.4º (220) and 75.2º (215) for both TiO_2 and Ag-TiO_2. Ag (200) is observed at 2θ 44.6º and 2θ 64.8º, while Ag (311) is detected at 2θ 77.475º (JCPDS 04-0783) for the AgNPs sample. AgO (200) at 2θ 32.2º (JCPDS 043-1038) could be observed for AgNPs. This implies that the AgNPs formed have a mixture of metallic Ag and AgO. It was also found that Ag(111) at 2θ 38.1º overlaps with TiO_2 (004) anatase, indicating the deposition of Ag onto TiO_2 for the composite samples.

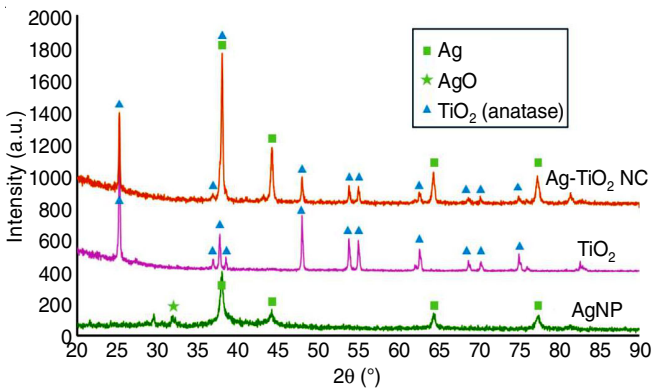

Fig. 5. XRD spectra of AgNPs, TiO_2 and Ag-TiO_2 NC

UV-Vis DRS was used to analyze changes in the light adsorption range and band gap energy (E_g) (Fig. 6). TiO_2 and Ag-TiO_2 NC showed sharp UV absorption edges at about ~340 nm, with Ag-TiO_2 having the highest adsorption edge. Nevertheless, it was observed that in comparison to TiO_2, Ag-TiO_2 NCs showed higher visible light adsorption (> 400 nm). This phenomenon may be attributed to the SPR effect exhibited by plasmonic Ag, as reported in a previous study [35]. Furthermore, a Kubelka-Munk plot was derived and revealed that the deposition of Ag

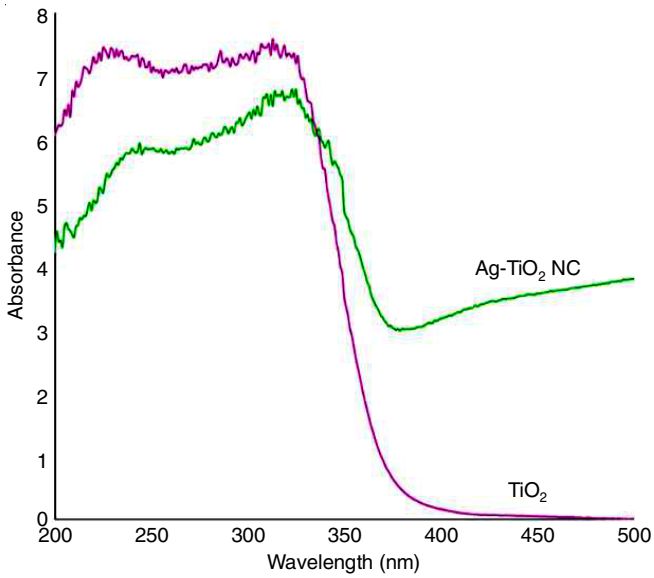

Fig. 6. UV-Vis DRS spectra of TiO_2 and Ag-TiO_2 NC

resulted in a reduced E_g from 3.05 eV (TiO_2) to 2.65 eV (Ag-TiO_2 NC, Fig. 7). The PL analysis revealed that TiO_2 exhibits significantly higher emission intensity at approximately 416 nm compared to the green-synthesized Ag-TiO_2 NC (Fig. 8). This is commonly observed in TiO_2 because of indirect band-to-band recombination or the recombination of self-trapped excitations within TiO_2 [36,37]. The substantial decrease in the PL emission spectra of Ag-TiO_2 NC could be attributed to the slow recombination rate facilitated due to the presence of Ag. This is plausible as Ag tends to act as an electron trap or charge carrier, creating a Schottky barrier at the interface with TiO_2 [38]. Furthermore, Fauzian *et al*. [39] reported that the lower Fermi energy level of Ag compared to TiO_2 reduces the band gap of TiO_2, enhancing charge separation and preventing electron-hole recombination within the TiO_2 crystal lattice.

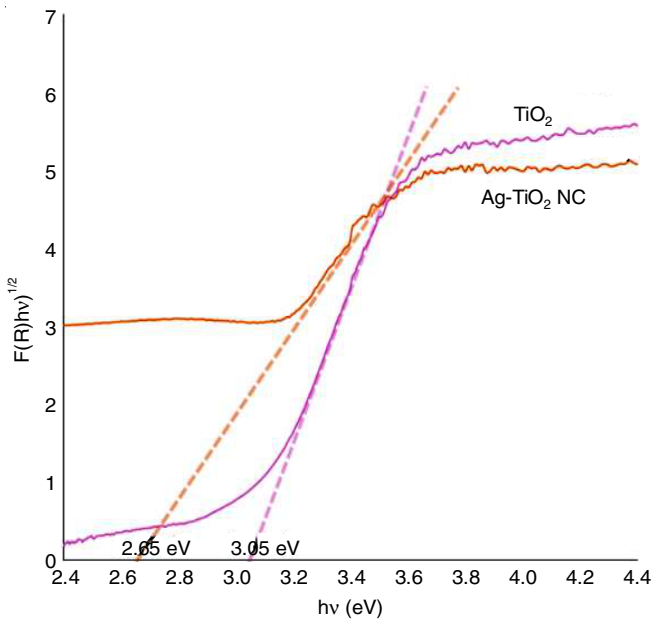

Fig. 7. Kubelka-Munk plot of diffuse reflectance spectra for TiO_2 and Ag-TiO_2 NC

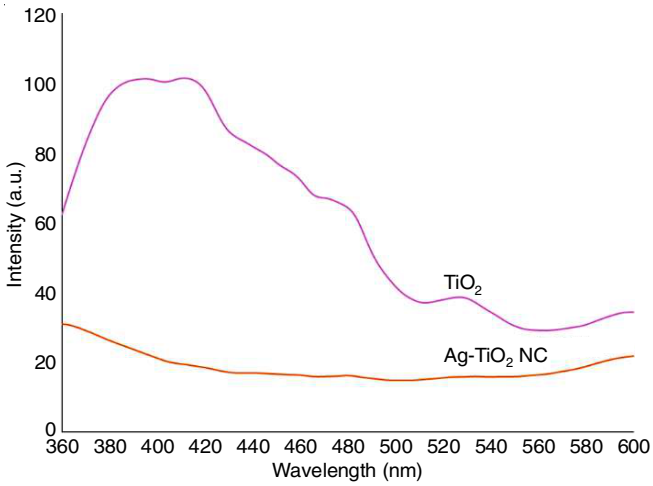

Fig. 8. PL spectra of TiO_2 and Ag-TiO_2 NC

Photocatalytic experiments

Control experiments: The photocatalytic activity of Ag-TiO_2 NCs was compared to the blank samples (TiO_2 and AgNP) under both UV and visible light. Fig. 9 illustrates that both AgNPs and TiO_2 have similar degradation rates of 95.1% and 94.4% for 5 ppm MB dye after 120 min under UV light. In comparison, Ag-TiO_2 NC demonstrates an enhanced photo-degradation of up to 99.6% under similar conditions. The enhanced photocatalytic performance of Ag-TiO_2 can be linked to the ability of Ag to act as an electron trap or charge carrier [35]. This minimizes electron-hole recombination in TiO_2, as evidenced by the photoluminescence (PL) analysis, due to the movement of free electrons within the crystal lattice. In comparison to the photocatalytic performance under UV light, MB was only removed at 7.3% by TiO_2 under visible light. TiO_2 only has an effective absorbance range within the UV region [40]. This is due to their high energy band gap (E_g = 3.05 eV) as depicted through UV-Vis DRS. However, Ag-TiO_2 NC showed remarkable photocatalytic ability under visible light with MB removal of 64.3%, likely due to the SPR effects of plasmonic Ag allowing for a wider range of light absorption [41].

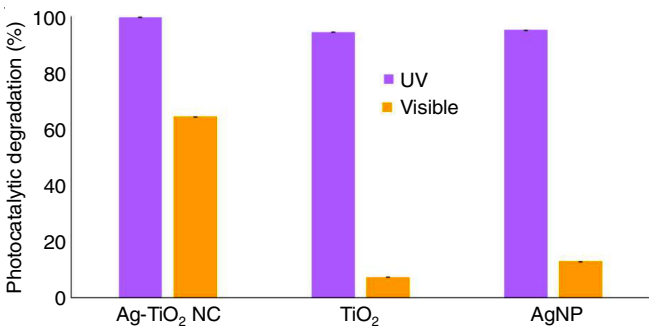

Fig. 9. Degradation efficiency (%) of methylene blue removal by Ag-TiO_2 NC, AgNPs and TiO_2 under UV and visible lights

Effect of parameters

Effect of dosage: Various dosages of Ag-TiO_2 NCs (0.1 to 1.0 g/L) were used to determine the best amount of Ag-TiO_2 to degrade MB (Fig. 10). The photocatalytic activity for

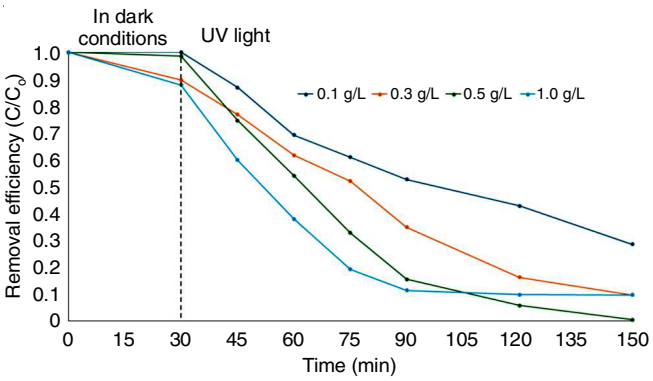

Fig. 10. Degradation efficiency (%) of methylene blue with respect to different dosages of Ag-TiO_2 NC

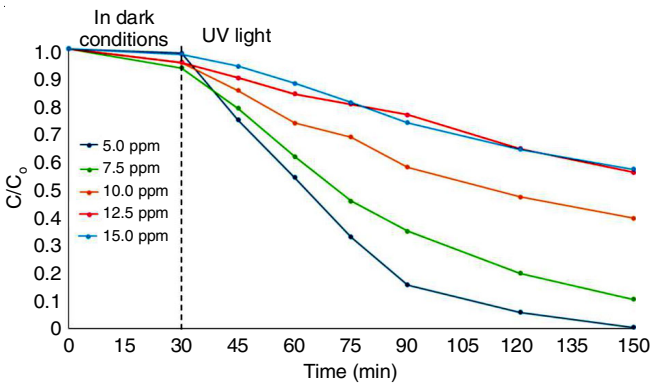

Fig. 11. Degradation efficiency (%) of methylene blue with respect to initial concentration of methylene blue

degradation of MB at a fixed concentration of 5 ppm increases as the dosage of Ag-TiO_2 rises from 0.1 to 0.5 g/L. However, once the dosage doubled to 1.0 g/L, a slight decrease in the photocatalytic ability to degrade MB is observed. This is because increasing the dosage of Ag-TiO_2 NC allows for more active sites that could absorb photons from UV light and MB dye molecules on the surface of the photocatalyst, which would result in the generation of more HO$^\bullet$ radicals [42]. Nevertheless, an excessive amount of Ag-TiO_2 NC could weaken the photocatalytic efficiency. This is because of the increased turbidity of the solution, which reduces light penetration and further hinders the photocatalytic process [13].

Effect of initial concentration: The impact of initial concentration on the photocatalytic degradation rate of MB was studied by using various concentrations of MB, with a constant dosage of 0.5 g/L Ag-TiO_2 NC (Fig. 11). An increase in the initial concentration of MB dye is associated with a reduction in its removal rate. The effect of initial MB concentrations follows the apparent pseudo-first-order kinetics (Table-2). The higher removal observed at the initial concentration of 5 ppm is likely attributed to adequate light penetration in the aqueous medium, enabling photon adsorption from the UV light onto the surface of the Ag-TiO_2 NCs. However, at higher initial concentrations, the reduction of the photocatalytic degradation of MB is likely due to the concentrated MB solution that reduced the penetration of light into the solution [43]. Furthermore, at lower concentrations, the Ag-TiO_2 surface is not saturated with MB molecules, hence allowing for more reactive sites on the Ag-TiO_2 NC surface to produce HO$^\bullet$ radicals [44]. At elevated concentrations, the surface of Ag-TiO_2 NC would be saturated with MB molecules that adsorb the light and photons causing deactivation of the photocatalytic degradation reaction. This occurs because the photons from the UV irradiation do not reach the surface of the Ag-TiO_2 NC, thereby hindering the production of HO$^\bullet$ radicals [38].

The influence of the initial MB dye concentration on the photocatalytic degradation rate was further analyzed using the Langmuir-Hinshelwood (L-H) kinetics model to account for the reactions occurring at the solid-liquid interfaces between Ag-TiO_2 and MB aqueous suspension (Fig. 12a-b). The plot of $1/K_{ph}$ against initial concentration gave a straight line with a high regression coefficient, $R^2 = 0.954$. The values of K_1 and K_2 were determined for the slope of the equation ($1/K_1$) and the intercept ($1/K_1K_2$). The values of K_1 (which represents the photocatalytic reaction rate constant) and K_2 (which represents the adsorption rate constant) are 0.0432 L/g and 0.2395 g/Lmin^{-1}. The product K_1K_2, which represents the apparent K_{ph}, is 0.0103 min^{-1}. The K_{app} obtained from the L-H kinetic model agrees with the experimental data obtained based on the L-H equation for photocatalysis at lower concentrations. Hence, the L-H kinetic model is suited to represent the photocatalytic degradation of MB by Ag-TiO_2 NC.

TABLE-2
KINETIC PARAMETERS OF PHOTOCATALYTIC DEGRADATION OF MB IN AQUEOUS SOLUTION AS A FUNCTION OF INITIAL CONCENTRATION

Initial concentration (ppm)	Rate constant, K_{ph} (min^{-1})	Regression coefficient, R^2
5.0	0.0395	0.9067
7.5	0.0174	0.9833
10.0	0.0073	0.9931
12.5	0.0045	0.9863
15.0	0.0043	0.9910

Effect of mixed dye solutions: To provide insight into the ability of Ag-TiO_2 NC to treat actual dye-polluted waters, a study was done to elucidate its photocatalytic performance to degrade cationic dyes, MB and RhB and anionic dyes, CR and MO individually and in a mixed dye system. This is because dye-tainted effluents often comprise a wide spectrum of dyes and studying the ability of a photocatalyst to degrade a singular dye limits the comprehension of its application in actual wastewater treatment.

For both studies against individual and mixed dye solutions, 0.5 g/L of Ag-TiO_2 NC was used with concentrations of each dye at 5 ppm. All samples that were treated with the photocatalyst were irradiated under UV light for 120 min, with the first 30 min being in the dark. It was observed that in comparison to cationic dyes RhB and MB, anionic dyes MO and CR exhibited higher adsorption in dark for individual dye samples (Fig. 13a). CR had a substantially higher adsorption rate with a removal efficiency of 75.5% removal in dark. However, in comparison to CR, removal by adsorption in the dark for MO was only 7.7%. The higher adsorption rate of anionic dyes is a result of the high concentration of positive charge of the nanocomposite allowing attraction and binding of negatively

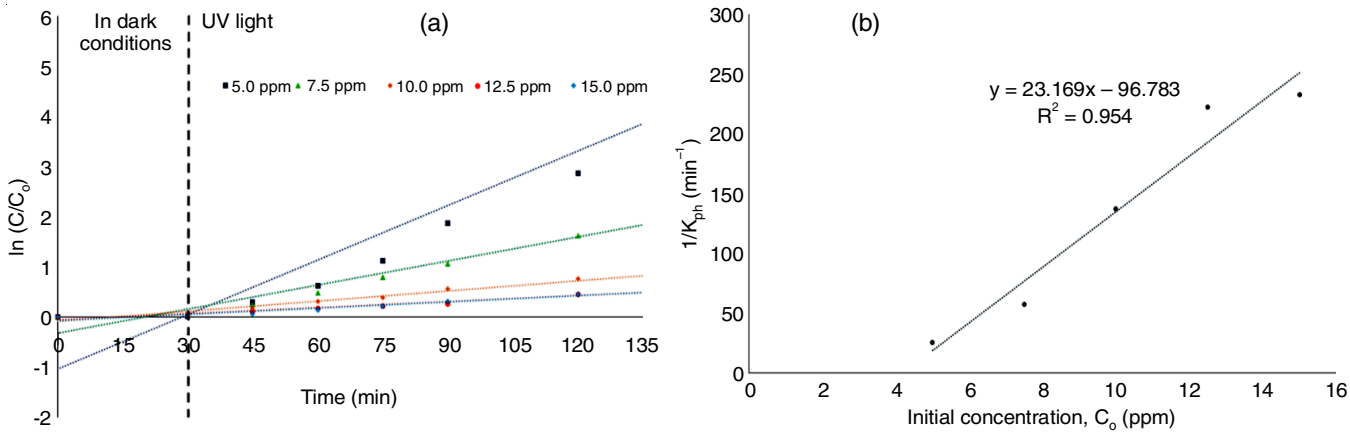

Fig. 12. Pseudo-first order kinetics for the degradation of MB with different initial concentrations (a) and Langmuir-Hinshelwood (LH) kinetics model for the photodegradation of methylene blue by Ag-TiO_2 NC (b)

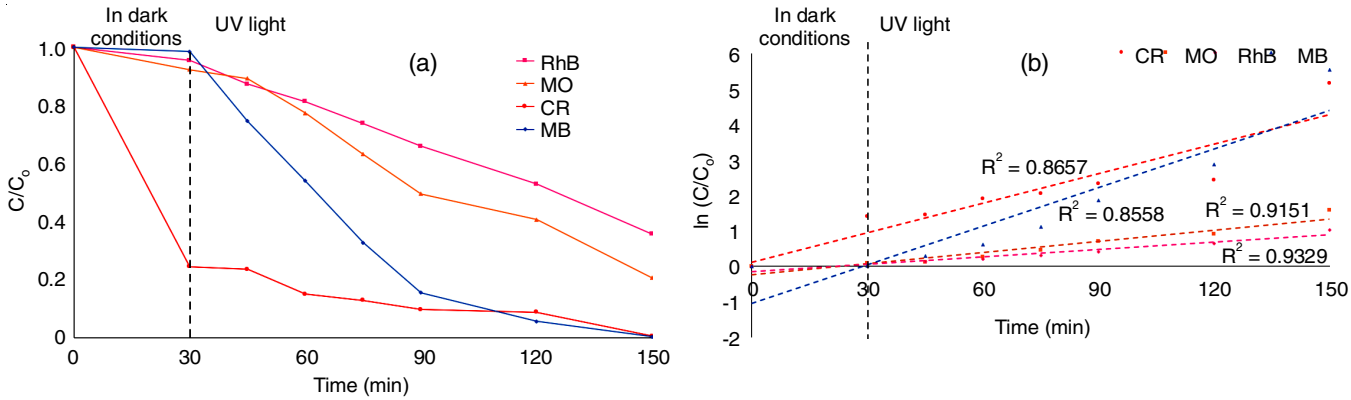

Fig. 13. Photocatalytic degradation of individual dyes MB, RhB, MO and CR (a) and pseudo-first order kinetics for the degradation of individual dyes (b)

charged CR and MO molecules to the active sites of Ag-TiO_2 [45,46]. Moreover, the molecular structure of CR is inherently different as it possesses more than one negatively charged sulfonate group in comparison to MO which allows for better electrostatic interaction between the photocatalyst and CR. Nevertheless, the removal of CR by adsorption in dark was not complete and a study on the photoactivity of CR was still possible.

The overall photodegradation of individual dyes showed that MB had the highest degradation rate at 99.6%, followed by CR, MO and RhB at 99.4%, 79.3% and 64.3%, respectively (Fig. 13a-b). The disparity in the degradation rates of anionic dyes CR and MO arises from their electrostatic interaction with electropositive clusters, enabling more efficient adsorption than with cationic dyes such as RhB [47]. Nevertheless, the high degradation of MB in comparison to the other dyes is mainly attributed to its simpler molecular structure in comparison to the other three dyes.

Currently, most of the photocatalytic photocatalysis studies involving green synthesized nanomaterials only evaluate the material's efficiency in acting against single dyes or pollutants [18-22]. Therefore, equimolar amounts of the four dyes were mixed to further investigate the photocatalytic degradation process in mixed dye solutions. The removal rates of all the dyes in mixed system were completely different in comparison to their counterparts (Fig. 14a-b). It was observed that the removal rate of all the dyes was the opposite, with RhB being the highest at 91.6%, followed by MO, CR and finally MB at 83.7%, 82.5% and 59.4% respectively (Fig. 14a-b). Moreover, the kinetic rate constant for the removal of the dyes for MB and CR dropped from 0.0362 min^{-1} and 0.0277 min^{-1} to 0.0069 min^{-1} and 0.0111 min^{-1}, while the rate constant for the degradation of MO and RhB increased from 0.0105 min^{-1} and 0.0069 min^{-1} to 0.0145 min^{-1} and 0.0121 min^{-1} (Table-3). The reduction of MB removal in comparison to the other dyes could be due to the selective adsorption of the anionic dyes which interferes with the ability of Ag-TiO_2 NCs to degrade MB efficiently despite having a better degradation rate as a single dye [48]. Furthermore, the enhanced degradation of RhB could have been caused by the adsorption of anionic dyes MO and CR, which results in better adsorption of RhB as a result of π-π stacking, hence enhancing the removal rate of these three dyes altogether [49-51].

Fig. 15 illustrates the UV-Vis time profile for the photocatalytic degradation of mixed and individual dyes. It can be observed that as time progresses, the intensity of the absorption peaks for all solutions gradually decreases for both mixed dyes (Fig. 15a) and individual dyes CR (Fig. 15b), MO (Fig. 15c), RhB (Fig. 15d) and MB (Fig. 15e). The peak at 664 nm can be ascribed to the dimethylamine group and thiazine group of

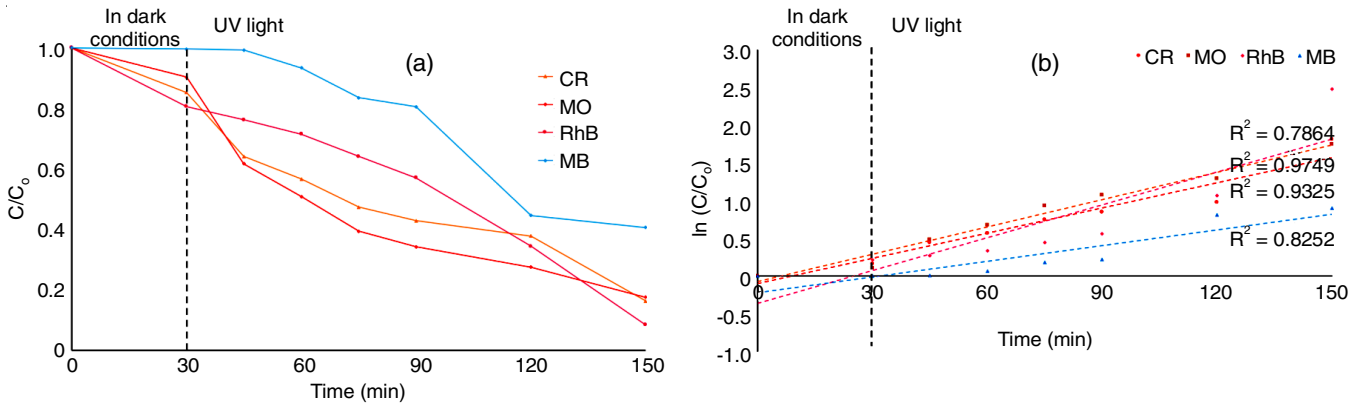

Fig. 14. Photocatalytic degradation of mixed dye solutions (a) and pseudo-first order kinetics for photodegradation of mixed dyes (b)

TABLE-3
KINETIC PARAMETERS FOR THE PHOTOCATALYTIC DEGRADATION OF INDIVIDUAL DYES AND MIXED DYE SYSTEM

Nature of dye	Dye	Rate constant, K_{ph} (min^{-1})		Regression coefficient, R^2	
		Individual	Mixed	Individual	Mixed
Cationic	MB	0.0362	0.0069	0.8657	0.8252
	RhB	0.0069	0.0121	0.9151	0.7864
Anionic	CR	0.0277	0.0111	0.8558	0.9325
	MO	0.0105	0.0145	0.9329	0.9749

MB molecules. In case of both mixed and individual dyes, these chromophore groups exhibited conjugation loss at the λ_{max}. This is likely to be caused by N-demethylation and deamination of MB dye molecules [52]. On the other hand, for both MO and CR, the azo groups (-N=N-) in these molecules were degraded, as indicated by their characteristic peaks at 464 nm and 490 nm in both mixed and individual dye samples. Absorption peaks for CR at ~350 nm which is assigned to biphenyl aromatic rings showed a very noticeable decrease in its peak showing that aromatic compounds were broken down in the degradation process [53]. Finally, RhB the chromophore structures of the N-ethyl groups on the sides of the xanthene rings were ascribed to absorption peak at 564 nm. This corresponds to the n→π transition of C=N and C=O groups. It can be seen that similarly to MB, RhB was degraded through the cleavage of chromophore groups, followed by hydroxylation, aromatic ring opening and mineralization of the overall compound [54].

So, the performance of Ag-TiO_2 NC showed a reliance on the photodegradation process towards the affinity of the photocatalyst to absorb dye molecules of different natures. While MO and RhB did not show much degradation when treated individually in comparison to CR and MB, it was revealed that in mixed dye solutions, the degradation process was substantially improved due to the selective interaction of the photocatalyst with other dyes. This shows the potential of plant extract mediated green synthesis as a feasible method to realistically dye-laden effluents.

Antibacterial study: The antibacterial study aimed to assess the effectiveness of Ag-TiO_2 synthesized through onion peel extract in producing a photocatalyst with antibacterial activity against Gram-positive bacteria, *E. coli* and Gram-negative bacteria, *S. aureus,* respectively. A control test was performed to compare the effectiveness of each component (onion peel extract, TiO_2, AgNP and Ag-TiO_2 NC) with a fixed concentration of 1 g/L against both bacterial samples (Fig. 16).

It can be observed that each component has varying mechanisms that play a role in inhibiting bacterial growth. It was observed that both Gram-negative and Gram-positive bacterial samples demonstrated significant antibacterial properties, with onion peel extract and AgNPs playing a key role in the green-synthesized Ag-TiO_2 NC. The onion peel extract and AgNPs showed high inhibition zones at 12.55 ± 0.39 mm and 14.80 ± 0.30 mm for *E. coli* (Fig. 16). Comparatively, bare TiO_2 samples showed limited activity against *E. coli*. Most studies stated that the primary mode of action for TiO_2 is the production of reactive oxygen species, while its larger particle size poses challenges for cell membrane penetration [55,56]. However, the Ag-TiO_2 NC displayed a larger inhibition zone at 13.01 ± 1.97 mm. This is attributed to the small size AgNPs, which enables them to penetrate cell walls and membranes, along with the bioactive compounds present in the onion peel extract [30,57]. Similar activities were also observed against *S. aureus*. The only difference between the two samples is that TiO_2 is shown to have antibacterial properties against the Gram-negative bacteria. This could be a result of the positively charged TiO_2, which can attract the negatively charged teichoic acids in the peptidoglycan resulting in surface interactions of TiO_2 with the cell membrane of *S. aureus*. The difference in the ability of Ag-TiO_2 NC to inhibit the growth of *E. coli* compared to *S. aureus* can be attributed to the structural differences between Gram-negative and Gram-positive bacteria. Gram-negative bacteria possess a thicker peptidoglycan layer, which acts as a barrier, making it more challenging for Ag-TiO_2 NC to penetrate the cells compared to Gram-positive bacteria [58].

Additional studies were conducted to evaluate the influence of Ag-TiO_2 NC dosage on inhibiting the growth of bacterial

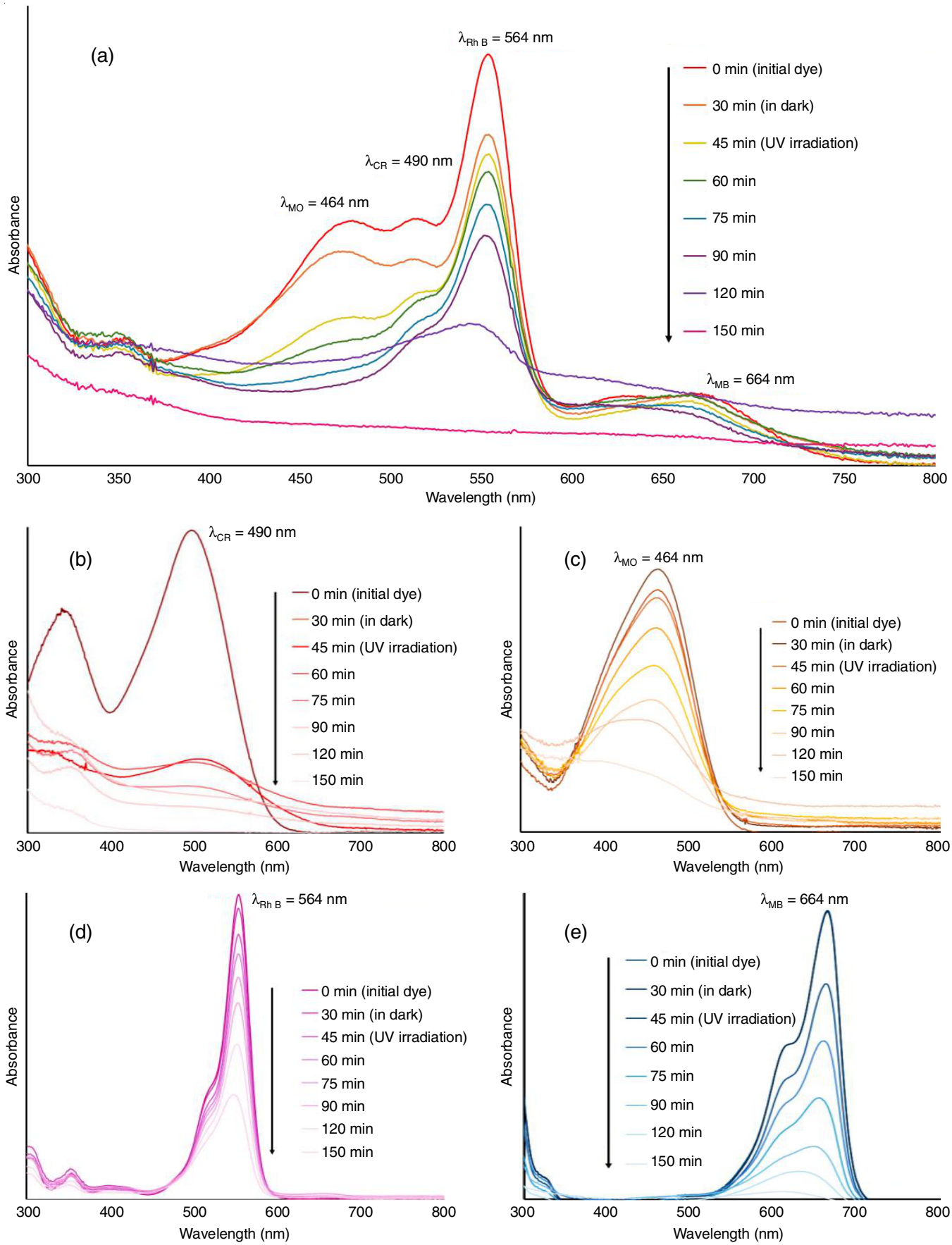

Fig. 15. UV-Vis absorption spectra of (a) mixed dye solutions (MB, RhB, MO and CR) and individual dyes (b) CR, (c) MO, (d) RhB and (e) MB

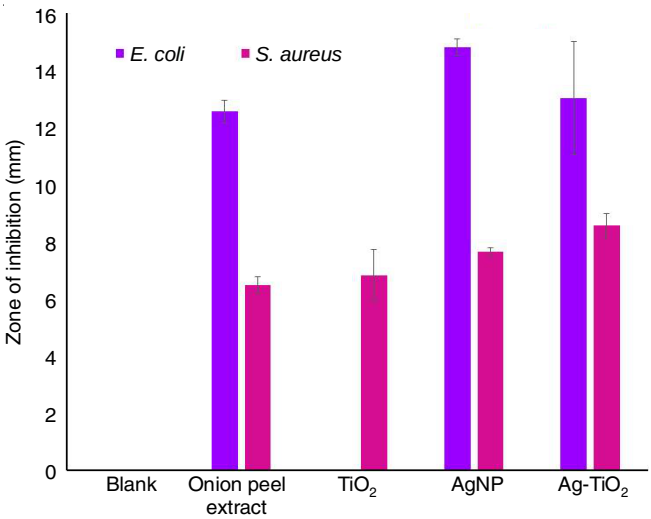

Fig. 16. Inhibition zones (mm) and antibacterial activity against *E. coli* and *S. aureus*

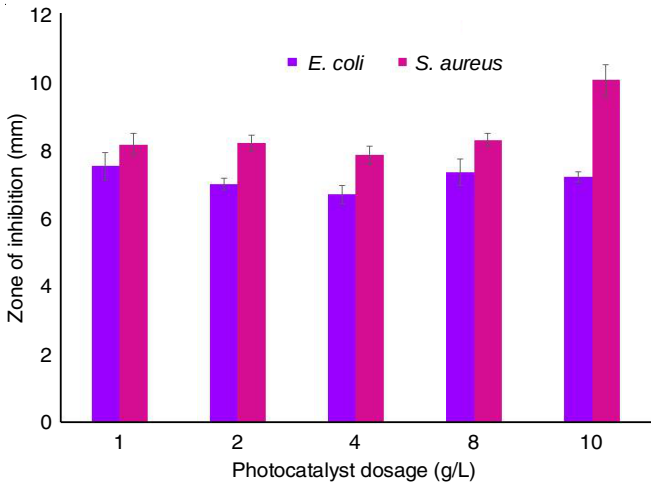

Fig. 17. Inhibition zones (mm) and antibacterial activity by different photocatalyst dosages against *E. coli* and *S. aureus*

samples (Fig. 17). It was found that for *E. coli*, an increase in concentration from 1 g/L to 10 g/L showed no significant increase in the inhibition zone. This trend suggests a saturation point where the maximum antimicrobial effect was achieved. The plateau effect can be explained by the limited interaction between the nanomaterials and bacteria beyond a certain concentration and once saturated, further increase in Ag-TiO_2 NC does not pro-portionally enhance the antimicrobial activity. Consequently, for *S. aureus*, the increase in concentration of Ag-TiO_2 NC from 1 g/L to 10 g/L increased in the inhibition zone. This could mean that a higher concentration of nanomaterials is needed for a more effective disruption of bacterial activities as Gram-negative bacteria possess a thicker peptidoglycan layer as opposed to Gram-positive bacteria. This study reveals that green synthesized Ag-TiO_2 NC holds promise as an antimicrobial agent for use in the water treatment processes.

Stability of Ag-TiO_2 NC: Despite the remarkable ability of the green synthesized Ag-TiO_2 NC to nearly complete catalyze different dyes, its photostability and recyclability must be considered to ensure functionality after multiple uses. Hence, MB was chosen to determine the stability given the high degradation rate. The photocatalytic degradation of MB after four consecutive photocatalytic cycles under optimized conditions was studied (Fig. 18). The efficiency for the photodegradation of MB by Ag-TiO_2 NC showed a slight reduction from 97.8% to 72.5% after 4 cycles. The reduction in photocatalytic ability could be due to certain changes after a few cycles of photocatalysis. As shown in the SEM micrograph (Fig. 19), the recovered Ag-TiO_2 NC agglomerated after four consecutive runs. This could have caused low radiation penetration inside the agglomerates, hence resulting in reduced photocatalytic activity.

However, the elemental mapping with EDX (Table-4) revealed a slight reduction in Ag and Ti mass percentage. Further

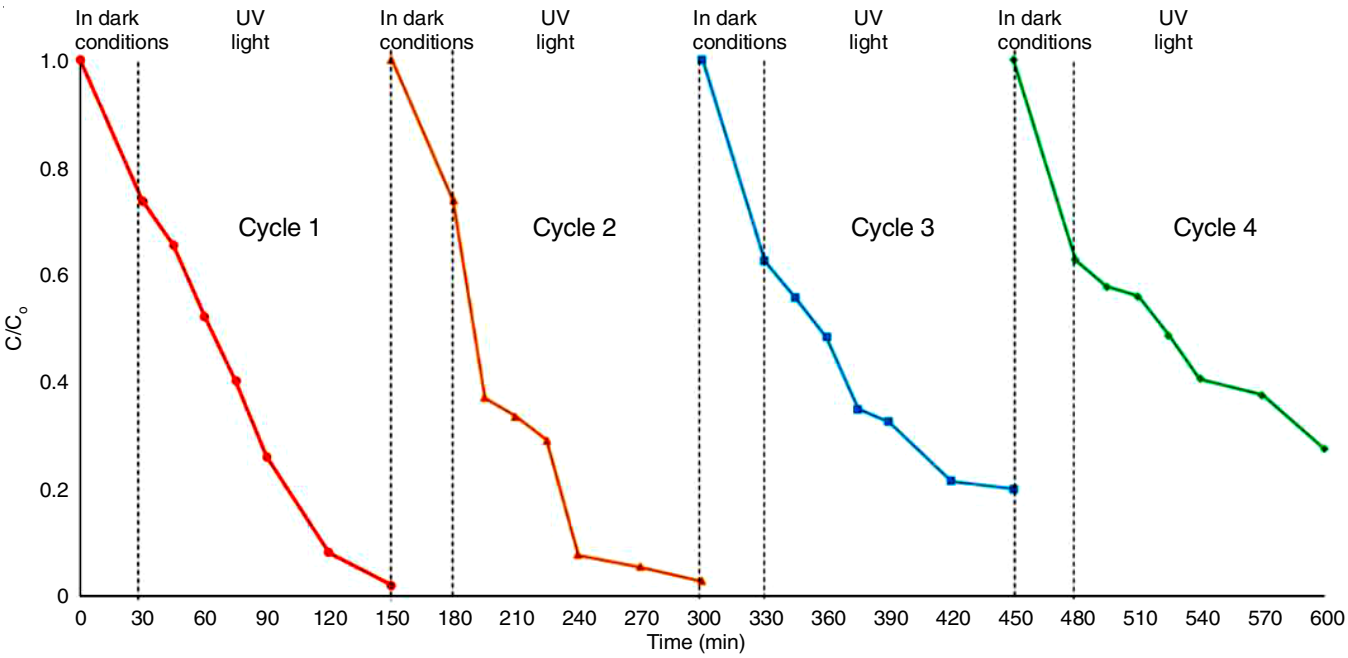

Fig. 18. Recyclability study of Ag-TiO_2 NC

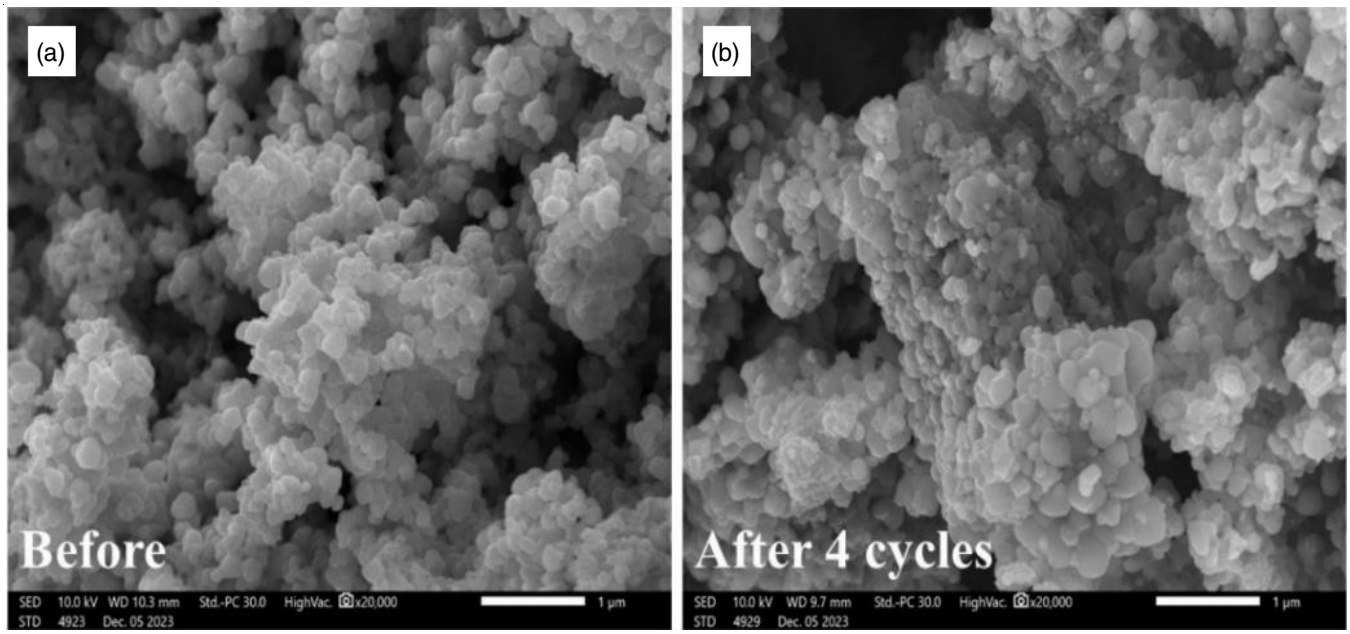

Fig. 19. SEM micrographs of Ag-TiO_2 NC before (a) and after 4th recycling (b)

TABLE-4
ELEMENTAL COMPOSITION OF Ag-TiO_2 NC BEFORE AND AFTER THE 4th CYCLE

Elements	Mass percentage (%)	
	Before	After
O	23.94 ± 0.05	30.11 ± 0.06
Ti	39.47 ± 0.18	36.32 ± 0.04
Ag	36.59 ± 0.16	33.57 ± 0.05
Total	100.00	100.00

analysis was also performed using XRD (Fig. 20), which showed no differences in the crystal structure of Ag-TiO_2 NC before and after recycling. All the major peaks for anatase phase TiO_2 and Ag are present in the XRD spectra. The findings indicate that the crystal form of the photocatalytic material was not destroyed over the process. Hence, this study provides a notable insight into the ability of green synthesis through plant extract-induced reactions to form exceptionally stable photocatalytic materials.

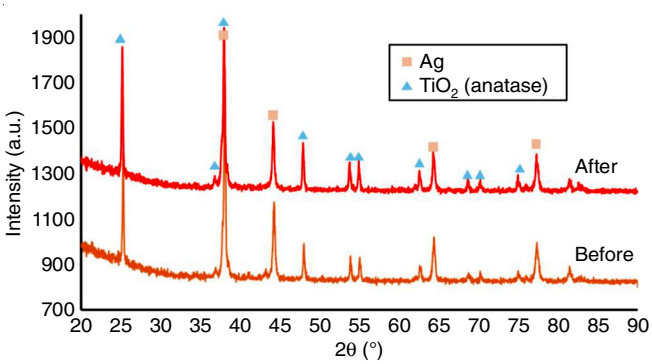

Fig. 20. XRD spectra before (a) and after 4th recycling (b) of Ag-TiO_2 NC

Proposed degradation pathway: The photocatalytic mechanism of a semiconductor begins with the generation of electron-hole pairs in the conduction band (e^-_{cb}) and the valence band (h^+_{vb}) when exposed to UV light. The elucidation of the photocatalytic mechanism was carried out by introducing the radical scavengers to the aqueous system containing the MB pollutant. This was conducted to determine the main reactive species responsible for the degradation of MB. Fig. 21a illustrates that the order of MB removal efficiency using Ag-TiO_2 NC in the presence of the radical scavengers is BZQ (80.1%) > MeOH (59.4%) > H_2O_2 (59.2%). The removal efficiency is significantly higher in the absence of scavenging agents, indicating that $^{\bullet}O_2^-$ radicals are not a prominent component in the photocatalytic degradation mechanism. Conversely, the presence of MeOH and H_2O_2 significantly reduced the degradation efficiency to 59.4% and 59.2%, suggesting that $^{\bullet}OH$ and h^+ are the predominant species responsible for the degradation of MB.

As shown in Fig. 21b, the photocatalytic activity of Ag-TiO_2 NC is initiated by the irradiation of UV light. This causes the valence band (VB) electron in TiO_2 to be at its highest energy state, thus causing an increase in the potential energy of the electron. The electrons will then be further excited, resulting in the migration of the electrons from TiO_2 into Ag. As demonstrated through PL analysis and UV-DRS, the incorporation of Ag led to a reduction of band gap (E_g) and electron-hole recombination. This indicates that Ag effectively served as an electron trap, facilitating the formation of electron-hole pairs in the process (eqn. 1). The electrons from Ag lead to the formation of $^{\bullet}O_2^-$ radicals, which then react with H_2O molecules to produce the main reactive species, $^{\bullet}OH$ radicals responsible for the degradation of MB (eqns. 2-3). Subsequently, the photogenerated holes can react with H_2O to produce $^{\bullet}OH$ (eqn. 4) and subsequently lead to the production of degradation products (eqn. 5). The findings of this study align with the reported studies [59], which identified holes as the main reactive species involved in the photocatalytic reaction mechanisms. The photocatalytic mechanism for MB degradation by Ag-TiO_2 NC is summarized as follows:

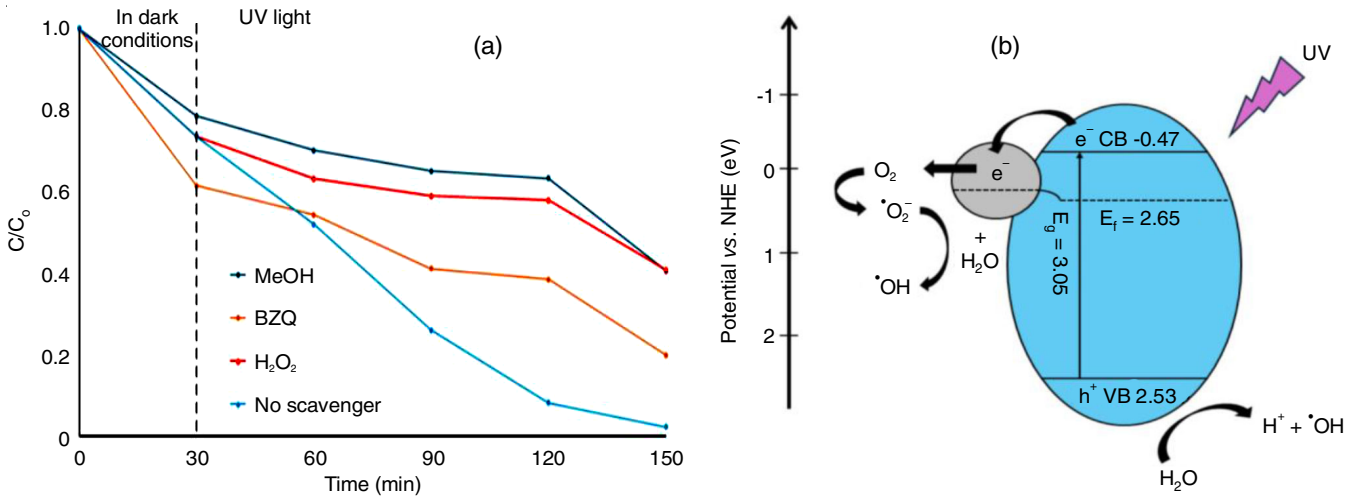

Fig. 21. Effect of reactive species on methylene blue photodegradation using Ag-TiO_2 NC and the schematic illustration of the proposed photocatalytic mechanism of Ag-TiO_2 NC (b)

$$\text{Ag-TiO}_2 + h\nu \rightarrow \text{Ag-TiO}_2(e^- + h^+) \quad (1)$$

$$e^- + O_2 \rightarrow {}^{\bullet}O_2^- \quad (2)$$

$$H_2O + {}^{\bullet}O_2^- \rightarrow OH^- + {}^{\bullet}OH \quad (3)$$

$$\text{Ag-TiO}_2(h^+) + H_2O \rightarrow H^+ + {}^{\bullet}OH \quad (4)$$

$${}^{\bullet}OH + MB \rightarrow CO_2 + H_2O \text{ (degradation products)} \quad (5)$$

Conclusion

This study emphasizes the potential of microwave-assisted synthesis approach for producing Ag-TiO_2 NCs as an effective agent for water remediation. The green synthesized Ag-TiO_2 NC showed stable formation of AgNPs with enhanced charge separation and reduced energy band gap, which allows for photonic absorption under visible light and thus outperforms the photocatalytic performance of TiO_2 under UV-visible light. Under UV-visible light, Ag-TiO_2 NC was able to degrade 5 ppm of MB dye almost completely with a degradation efficiency of 99.6% and 64.3% within 150 min of treatment time. In addition, the green synthesized Ag-TiO_2 also showed affinity towards the adsorption of anionic dyes CR and MO individually and showed remarkable removal of both anionic dyes and cationic dyes in the mixed dye solutions. The Ag-TiO_2 NC also showed promising stability with a slight reduction in the photocatalytic ability to degrade MB from 97.9% to 72.6% after 4 consecutive treatment cycles. Moreover, the antibacterial assay revealed that the green synthesized Ag-TiO_2 showed enhanced antibacterial properties against both *E. coli* and *S. aureus* in comparison to bare TiO_2 due to the deposition of Ag as well as the presence of bioactive compounds from the onion peel extract, which acts as a potent antibacterial agent in the synthesized NC. Hence, the green synthesized Ag-TiO_2 NCs reveals the potential of plant extract, in this case, a waste material, in mediating the synthesis of photocatalytic nanomaterials without the need for harsh solvents and chemicals. This provides a more sustainable alternative in attaining functional and highly stable photocatalytic nanomaterials, as plant materials are abundantly found from a wide array of sources.

ACKNOWLEDGEMENTS

The authors acknowledge Universiti Malaysia Sarawak for funding this study under the Vice Chancellor's High Impact Research Grant (UNI/F07/VC-HIRG/85506/P10-01/2022).

CONFLICT OF INTEREST

The authors declare that there is no conflict of interests regarding the publication of this article.

REFERENCES

1. P. Sharma, S. Pant, S. Rai, R.B. Yadav and V. Dave, *J Polym. Environ.*, **26**, 1795 (2018); https://doi.org/10.1007/s10924-017-1081-7
2. M. Munir, M.F. Nazar, M.N. Zafar, M. Zubair, M. Ashfaq, A. Hosseini-Bandegharaei, S. U.-D. Khan and A. Ahmad, *ACS Omega*, **5**, 16711 (2020); https://doi.org/10.1021/acsomega.0c01613
3. M. Berradi, R. Hsissou, M. Khudhair, M. Assouag, O. Cherkaoui, A. El Bachiri and A. El Harfi, *Heliyon*, **5**, e02711 (2019); https://doi.org/10.1016/j.heliyon.2019.e02711
4. A. Tkaczyk, K. Mitrowska and A. Posyniak, *Sci. Total Environ.*, **717**, 137222 (2020); https://doi.org/10.1016/j.scitotenv.2020.137222
5. S. Dutta, S. Adhikary, S. Bhattacharya, S. Chatterjee, A. Chakraborty, D. Roy, D. Banerjee, A. Ganguly, S. Nanda and P. Rajak, *J. Environ. Manage.*, **353**, 120103 (2024); https://doi.org/10.1016/j.jenvman.2024.120103
6. N.Y. Donkadokula, A.K. Kola, I. Naz and D. Saroj, *Rev. Environ. Sci. Biotechnol.*, **19**, 543 (2020); https://doi.org/10.1007/s11157-020-09543-z
7. M. Ahmed, M.O. Mavukkandy, A. Giwa, M. Elektorowicz, E. Katsou, O. Khelifi, V. Naddeo and S.W. Hasan, *npj Clean Water*, **5**, 12 (2022); https://doi.org/10.1038/s41545-022-00154-5
8. F. Mashkoor and A. Nasar, *J. Magn. Magn. Mater.*, **500**, 166408 (2020); https://doi.org/10.1016/j.jmmm.2020.166408
9. D. Zamel and A.U. Khan, *Inorg. Chem. Commun.*, **131**, 108766 (2021); https://doi.org/10.1016/j.inoche.2021.108766
10. M.I. Din, R. Khalid, J. Najeeb and Z. Hussain, *J. Clean. Prod.*, **298**, 126567 (2021); https://doi.org/10.1016/j.jclepro.2021.126567
11. Z.-J. Zhao, S.H. Hwang, S. Jeon, B. Hwang, J.-Y. Jung, J. Lee, S.-H. Park and J.-H. Jeong, *Sci. Rep.*, **7**, 8915 (2017); https://doi.org/10.1038/s41598-017-09401-z

12. S. Ying, Z. Guan, P.C. Ofoegbu, P. Clubb, C. Rico, F. He and J. Hong, *Environ. Tech. Innov.*, **26**, 102336 (2022); https://doi.org/10.1016/j.eti.2022.102336
13. N. Sharma, K. Saszet, T. Szabó, D. Karajz, I.M. Szilágyi, S. Garg, Z. Pap and K. Hernadi, Catal. Today, **413-415**, 113984 (2023); https://doi.org/10.1016/j.cattod.2022.12.015
14. D. Bhardwaj and R. Singh, *Bioresour. Bioprocess*, **8**, 1 (2021); https://doi.org/10.1186/s40643-020-00357-z
15. M. Saeed, M. Muneer, M.K.K. Khosa, N. Akram, S. Khalid, M. Adeel, A. Nisar and S. Sherazi, *Green Process. Synth.*, **8**, 659 (2019); https://doi.org/10.1515/gps-2019-0036
16. R.A. Banjara, A. Kumar, R.K. Aneshwari, M.L. Satnami and S.K. Sinha, *Environ. Nanotech. Monit. Manag.*, **22**, 100988 (2024); https://doi.org/10.1016/j.enmm.2024.100988
17. X. Jiang, Z. Wang, X. Zhang, G. Jiang, Y. Peng, S.Xu, M. Cao, X. Dai, Z. Liu and J. Ma, J. *Nanopart. Res*., **21**, 211 (2019); https://doi.org/10.1007/s11051-019-4622-2
18. B. Kumar, K. Smita, Y. Angulo and L. Cumbal, *Green Process. Synth*., **5**, 371 (2016); https://doi.org/10.1515/gps-2016-0003
19. T. Mohapatra, S. Manekar, V.K. Sahu, A.K. Soni, S. Banerjee and P. Ghosh, *Int. J. Chem. React. Eng.*, **19**, 893 (2021); https://doi.org/10.1515/ijcre-2021-0111
20. T.H. Nguyen, N.H. Hoang, C.V. Tran, P.T.M. Nguyen, T.-D. Dang, W.J. Chung, S.W. Chang, D.D. Nguyen, P.S. Kumar and D.D. La, *Chemosphere*, **306**, 135474 (2022); https://doi.org/10.1016/j.chemosphere.2022.135474
21. P.C. Nethravathi, Udayabhanu, G. Nagaraju and D. Suresh, *Mater. Today: Proceed.*, **49**, 841 (2022); https://doi.org/10.1016/j.matpr.2021.05.670
22. F. Septiningrum, A.H. Yuwono, F.A. Maulana, E. Nurhidayah, D. Dhaneswara, N. Sofyan, H. Hermansyah and W.W. Purwanto, *Curr. Res. Sustain. Chem.*, **8**, 100394 (2024); https://doi.org/10.1016/j.crgsc.2023.100394
23. M. Marrelli, V. Amodeo, G. Statti and F. Conforti, *Molecules*, **24**, 119 (2018); https://doi.org/10.3390/molecules24010119
24. M. Kumar, M.D. Barbhai, M. Hasan, S. Punia, S. Dhumal, Radha, N. Rais, D. Chandran, R. Pandiselvam, A. Kothakota, M. Tomar, V. Satankar, M. Senapathy, T. Anitha, A. Dey, A.A.S. Sayed, F.M. Gadallah, R. Amarowicz and M. Mekhemar, *Biomed. Pharmacother.*, **146**, 112498 (2022); https://doi.org/10.1016/j.biopha.2021.112498
25. M.A. Abid, D.A. Abid, W.J. Aziz and T.M. Rashid, *Phys. B: Condens. Matter.*, **622**, 413277 (2021); https://doi.org/10.1016/j.physb.2021.413277
26. M.Z. Ahmad, A.S. Alasiri, J. Ahmad, A.A. Alqahtani, M.N. Abdullah, B.A. Abdel-Wahab, K. Pathak, R. Saikia, A. Das, H. Sarma and S.A. Alzahrani, *Molecules*, **27**, 7712 (2022); https://doi.org/10.3390/molecules27227712
27. P. Jegadeeswaran, P. Rajiv, P. Vanathi, S. Rajeshwari and R. Venckatesh, *Mater. Lett*., **166**, 137 (2016); https://doi.org/10.1016/j.matlet.2015.12.058
28. M. Jayapriya and M. Arulmozhi, Inorg. Chem. Commun., 128, 108529 (2021); https://doi.org/10.1016/j.inoche.2021.108529
29. W.M. Shume, H.C. Ananda Murthy and E.A. Zereffa, *J Chem.*, **2020**, 5039479 (2020); https://doi.org/10.1155/2020/5039479
30. T.N. Rao, Riyazuddin, P. Babji, N. Ahmad, R.A. Khan, I. Hassan, S.A. Shahzad and F.M. Husain, *Saudi J. Biol. Sci.*, **26**, 1385 (2019); https://doi.org/10.1016/j.sjbs.2019.09.005
31. F. Ahmed, M.B. Kanoun, C. Awada, C. Jonin and P.-F. Brevet, *Crystals*, **11**, 1488 (2021); https://doi.org/10.3390/cryst11121488
32. A. Joseph and A. Vijayanandan, *Sustain. Mater. Techmol*., **38**, e00703 (2023); https://doi.org/10.1016/j.susmat.2023.e00703
33. F. Tavakoli, A. Badiei and J.B. Ghasemi, *J. Water Environ. Nanotechnol*., **4**, 31 (2019); https://doi.org/10.22090/jwent.2019.01.003
34. X. Zhu, K. Pathakoti and H.M. Hwang, Green Synthesis of Titanium Dioxide and Zinc Oxide Nanoparticles and their Usage for Antimicrobial Applications and Environmental Remediation. In: Green Synthesis, Characterization and Applications of Nanoparticles, Elsevier, Chap. 10, pp. 223-263 (2019).
35. H. Chakhtouna, H. Benzeid, N.Zari, A.K. Qaiss and R. Bouhfid, *Environ. Sci. Pollut. Res.*, **28**, 44638 (2021); https://doi.org/10.1007/s11356-021-14996-y
36. D. Kanakaraju, F.D.A. Kutiang, Y.C. Lim and P.S. Goh, *Appl. Mater. Today*, **27**, 101500 (2022); https://doi.org/10.1016/j.apmt.2022.101500
37. N.F. Jaafar, A.A. Jalil, S. Triwahyono, J. Efendi, R.R. Mukti, R. Jusoh, N.W.C. Jusoh, A.H. Karim, N.F.M. Salleh and V. Suendo, *Appl. Surf. Sci*., **338**, 75 (2015); https://doi.org/10.1016/j.apsusc.2015.02.106
38. K. Tahir, A. Ahmad, B. Li, S. Nazir, A.U. Khan, T. Nasir, Z.H. Khan, R. Naz and M. Raza, *J. Photochem.Photobiol. B: Biol*., **162**, 189 (2016); https://doi.org/10.1016/j.jphotobiol.2016.06.039
39. M Fauzian, A Taufik and R Saleh, J. Phys.: Conf. Ser. 1725 012004 (2021); https://doi.org/10.1088/1742-6596/1725/1/012004
40. D. Li, H. Song, X. Meng, T. Shen, J. Sun, W. Han and X. Wang, *Nanomaterials*, 10, 546 (2020); https://doi.org/10.3390/nano10030546
41. Y. Chen, Y. Wang, W. Li, Q. Yang, Q. Hou, L. Wei, L. Liu, F. Huang and M. Ju, *Appl. Catal. B: Environ*., **210**, 352 (2017); https://doi.org/10.1016/j.apcatb.2017.03.077
42. D. Kanakaraju, M.A.A. Jasni, A. Pace and M.H. Ya, *Environ. Sci. Pollut. Res*., **28**, 68834 (2021); https://doi.org/10.1007/s11356-021-15440-x
43. A. Salama, A. Mohamed, N.M. Aboamera, T.A. Osman and A. Khattab, *Appl. Nanosci.*, **8**, 155 (2018); https://doi.org/10.1007/s13204-018-0660-9
44. Y. Li, S. Sun, M. Ma, Y. Ouyang and W. Yan, *Chem. Eng. J*., **142**, 147 (2008); https://doi.org/10.1016/j.cej.2008.01.009
45. S. Wang, F. Teng and Y. Zhao, *RSC Adv.*, **5**, 76588 (2015); https://doi.org/10.1039/C5RA14931B
46. A.P. Torane, A.B. Ubale, K.G. Kanade and P.K. Pagare, *Mater. Today: Proceed*., **43**, 2738 (2021); https://doi.org/10.1016/j.matpr.2020.06.476
47. M. S. Bootharaju and T. Pradeep, *Langmuir*, **29**, 8125 (2013); https://doi.org/10.1021/la401180r
48. M. Tang, R. Xu, Y. Gong, H. Zhang, J. He, P. Wu, C. Liu and W. Jiang, *Ind. Eng. Chem. Res*., **60**, 17520 (2021); https://doi.org/10.1021/acs.iecr.1c03958
49. B. Chen, F. Long, S. Chen, Y. Cao and X. Pan, *Chem. Eng. J*., **385**, 123926 (2020); https://doi.org/10.1016/j.cej.2019.123926
50. S.A. Ali, I.B. Rachman and T.A. Saleh, *Chem. Eng. J*., **330**, 663 (2017); https://doi.org/10.1016/j.cej.2017.08.003
51. I. Ali, S.A. AL-Hammadi and T.A. Saleh, *J. Mol. Liq.*, **269**, 564 (2018); https://doi.org/10.1016/j.molliq.2018.08.081
52. D. Kanakaraju, A.R.B. Reduan and Y.C. Lim, *J. Clust. Sci.*, **35**, 1063 (2024); https://doi.org/10.1007/s10876-023-02536-2
53. K. Liu, Y. Yang, F. Sun, Y. Liu, M. Tang and J. Chen, *Chemosphere*, **299**, 134417 (2022); https://doi.org/10.1016/j.chemosphere.2022.134417
54. N.T. Thao, H.T.P. Nga, N.Q. Vo and H.D.K. Nguyen, *J. Sci.: Adv. Mater. Device*, **2**, 317 (2017); https://doi.org/10.1016/j.jsamd.2017.07.005
55. J. Torres-Limiñana, A.A. Feregrino-Pérez, M. Vega-González, L. Escobar-Alarcón, J.A. Cervantes-Chávez and K. Esquivel, *Nanomaterials*, **12**, 1944 (2022); https://doi.org/10.3390/nano12111944
56. R. Hidayat, G. Fadillah, S.-I. Ohira, F.I. Fajarwati, D.A. Setyorini and A. Saputra, *Mater. Today Sustain*., **26**, 100752 (2024); https://doi.org/10.1016/j.mtsust.2024.100752
57. R.R. El Sadda, A.R. El-Shobaky, H.O. El Sharawy, E.A. Moawed, O.H. Gohar, M.M. El-Zahed, Y.Y. Elseady and W.S. El–Tohamy, *Process Biochem*., **147**, 587 (2024); https://doi.org/10.1016/j.procbio.2024.11.002
58. K.I. Dhanalekshmi, K.S. Meena and I. Ramesh, *Int. J. Nanotechnol. Appl*., **3**, 5 (2013).
59. T. Rahmawati, T. Butburee, W. Sangkhun, T. Wutikhun, J. Padchasri, P. Kidkhunthod, S. Phromma, T. Eksangsri, W. Kangwansupamonkon, P. Leeladee and C. Sapcharoenkun*Colloid Surf. A: Physiochem. Eng. Asp*., **665**, 131206 (2023); https://doi.org/10.1016/j.colsurfa.2023.131206